ISSN: 0798-1015

REVISTA ESPACIOS

Educación • Education • Educação • Vol. 41 (23) 2020 • Art. 16

Recibido/Received: 29/03/2020 • **Aprobado**/Approved: 01/06/2020 • **Publicado**/Published: 25/06/2020

Teaching the non-linear behavior of power electronic converters with *OpenModelica*

Enseñanza del comportamiento no lineal de convertidores electrónicos de potencia con *OpenModelica*

CANO-QUINTERO, Juan B. [1]
MUÑOZ-GALEANO, Nicolás [2]
LOPEZ-LEZAMA, Jesús M. [3]

Abstract
This paper presents a methodology for teaching the linearization process and non-linear behavior of Power Electronic Converters (PECs) through the OpenModelica Software. The methodology is based on a step-by-step approach consisting on the deduction of the large-signal and average models, linearization of the average model, deduction and analysis of transfer functions, deduction of steady state relationships and simulation with OpenModelica. The proposed teaching methodology is applied over an ideal DC/DC Boost converter analyzing its behavior in different operation points.
Key words: Power electronic converters, large-signal model, average model, OpenModelica

Resumen
Este artículo presenta una metodología para enseñar el proceso de linealización y el comportamiento no lineal de los convertidores electrónicos de potencia mediante el software OpenModelica. La metodología se basa en un enfoque paso a paso que consiste en la deducción de los modelos de gran señal y promedio, la linealización del modelo promedio, la deducción y el análisis de las funciones de transferencia, la deducción de las relaciones de estado estable y la simulación con OpenModelica. La metodología de enseñanza propuesta se aplica sobre un convertidor DC/DC Boost ideal analizando su comportamiento en diferentes puntos de operación.
Palabras clave: Convertidores de electrónica de potencia, modelo de gran señal, modelo promedio, OpenModelica

1. Introduction

Non-linear systems are complex and their linearization process tends to be complicated (Bi, Z. and Xia, W., 2010). Electrical and electronic engineering students usually have drawbacks to correctly understand and perform the linearization of Power Electronic Converters PECs. For this reason, this paper presents an easy and understandable methodology for performing the linearization process of PECs. Also, a step of the methodology

1 Docente del Departamento de Ingeniería Eléctrica, Facultad de Ingeniería, Universidad de Antioquia. Medellín, Colombia, email: bernardo.cano@udea.edu.co
2 Docente del Departamento de Ingeniería Eléctrica, Facultad de Ingeniería, Universidad de Antioquia. Medellín, Colombia, email: nicolas.munoz@udea.edu.co
3 Docente del Departamento de Ingeniería Eléctrica, Facultad de Ingeniería, Universidad de Antioquia. Medellín, Colombia, email: jmaria.lopez@udea.edu.co

for explaining the non-linear behavior of a PEC is included comparing the non-linear system with the linear one. The linear system behavior fits well to the non-linear behavior in the operation point; nevertheless, their differences are highlighted and explained.

PECs are inherently non-linear sine the differential equations that permits their modeling have, in some terms, the product of inputs and outputs (Yang and Liao, 2019). Usually, in the differential equations, the control signal is multiplied by any current or voltage of the system. So, the non-linearity is often introduced by the control signal. Control signal function is used commutate the power switch between on and off positions, so the switch is the PEC actuator and facilitates the operation of the PEC. Power switch permits the interchange of energy among the passive elements (inductors and capacitors) and the transfer of energy between the power source and the load (Muñoz-Galeano *et al*., 2019). Nevertheless, the commutation produces at least two commutation states when working in continuous condition mode and more than two states when working in discontinuous condition mode. This is the reason why converters feature a non-linear behavior and can be denominated as converters of variable structure.

Several papers have dealt with the analyses of PEC (Chamas *et al*, 2004; Hinz H *et al*, 2018; Rukun, 2018). Most of researchers in their analyses use any linearization technique and mainly focus on contributing in advanced control techniques and controllability analyses (Beldjajev, and Roasto, 2012; Davoudi *et al.*, 2013). So, they left behind the process of linearization and the explanation of the non-linear behavior of the converter. This paper describes in detail the process of linearization, the procedure in the deduction of equations and the basis of the non-linear behavior for PECs; all of these within a comprehensible step-by-step methodology. This facilitates the understanding of the non-linear behavior for PECs and the process of linearization (Raud Z., 2019). The proposed methodology can be used for students of power electronics curses and affine, and for researches that want to quickly obtain the information required for reading power electronic papers. For a better understanding, the methodology is applied for a boost DC/DC converter while results are focused on a deep explanation for its non-linear behavior. For the deduction of converter equations considering power losses, please consult (Muñoz-Galeano *et al*., 2019). For the sizing and tuning of controllers for converters, please consult (Urrea-Quintero, *et al.*, 2018).

2. Proposed methodology for teaching the non-linear behavior of DC/DC converters

This paper describes a methodology to teach the non-linear behavior and linearized modeling of PECs. The description is done for a DC/DC boost converter but can easily be applied to any other PEC. The aim of such description is to illustrate the different concepts of a linearized model for the PEC using not only a theoretical approach but also simulation to reinforce concepts. Special emphasis is done in identifying the differences between operation point and small signal variables from a practical point of view, using simulation, which allows identifying its implications on real PECs operation.

The proposed methodology includes the following steps: 1) Deduction of the large-signal model for the converter using circuital laws. 2) Deduction of the average model. 3) Linearization of the average model. 4) Deduction of transfer functions that depend on the operation point. 5) Analysis of transfer functions, using pole and zero location to predict their responses. 6) Deduction of steady state relationships between the operation point variables. 7) Simulations with OpenModelica software to validate the transfer functions and analyze the PECs behavior in different operation points.

2.1. Step 1: Deduction of the Large-signal model

Large-signal model purpose is to obtain a set of differential equations that permits the description of the inherent non-linear behavior of PECs. As stated before, the methodology is explained using the boost converter. Figure 1

shows the schematic diagram of a boost converter. It is composed of an input voltage source (v_i), a capacitor (C), an inductor (L), a load resistor (R), a diode (D) and a switching device (transistor) (Q). The switching device is controlled through a squared signal, using any Pulse Width Modulation (PWM) technique.

Figure 1
DC/DC Boost converter schematic

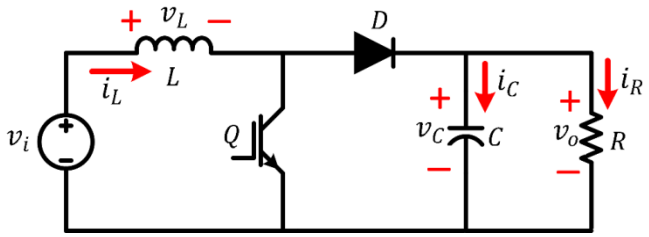

By using current and voltage conventions shown in fig. 1, it is possible to obtain the differential equations that model the boost converter. The two states of the switch Q are modeled by using the u variable where $u = 1$ and $u = 0$ are used to indicate that the switch is closed and open, respectively.

Applying Kirchhoff voltage and current laws for the circuit with Q open $(u = 0)$, equations (1) and (2) are obtained:

$$L\frac{di_L}{dt} = v_i - v_C \quad (1)$$

$$C\frac{dv_C}{dt} = i_L - \frac{v_C}{R} \quad (2)$$

Appling Kirchhoff voltage and current laws for the circuit with Q closed ($u = 1$), equations (3) and (4) are obtained:

$$L\frac{di_L}{dt} = v_i \quad (3)$$

$$C\frac{dv_C}{dt} = -\frac{v_C}{R} \quad (4)$$

Equations (1) to (4) can be resumed into equations (5) and (6) by considering both u values:

$$L\frac{di_L}{dt} = v_i \cdot u + (v_i - v_C)(1-u) \quad (5)$$

$$C\frac{dv_C}{dt} = -\frac{v_C}{R} \cdot u + (i_L - \frac{v_C}{R}) \cdot (1-u) \quad (6)$$

Equations (5) and (6) conforms the Differential Equations System (DES) that models the converter and is the starting point for obtaining the following linear models. This DES is named large-signal model because no assumptions are made regarding the magnitude of voltages and currents. This model allows observing all dynamics of PECs. The model is also called *switched model* since it includes the u signal in de equations. The u signal is discrete because it is limited to only two possible values (0 and 1) and it is also a discontinuous signal because its value changes instantaneously.

2.2. Step 2: Average model

The average model allows eliminating the fast dynamics using average values of system variables; it is used to obtain nominal values or values where the system is stabilized in the operation point. The discontinuous nature of the u signal affects voltages and currents of the converter. Inductor current (i_L) cannot become discontinuous because of the inductive effect that prevents sudden changes of this variable. An analog conclusion applies to capacitor voltage (v_C) due to the capacitive effect in which capacitor voltage cannot suddenly change. Instead, any other variable of the converter can present discontinuities. This is especially true for the first derivative of the inductor current (related to inductor voltage) and the first derivative of capacitor voltage (related to capacitor current). That is, i_L and v_C are continuous signals with discontinuous first derivatives (discontinuous slopes). In steady state, the discontinuity of i_L and v_C slopes can be visualized in signal ripple as shown in Figure 2.

Figure 2
Ripple of capacitor voltage output

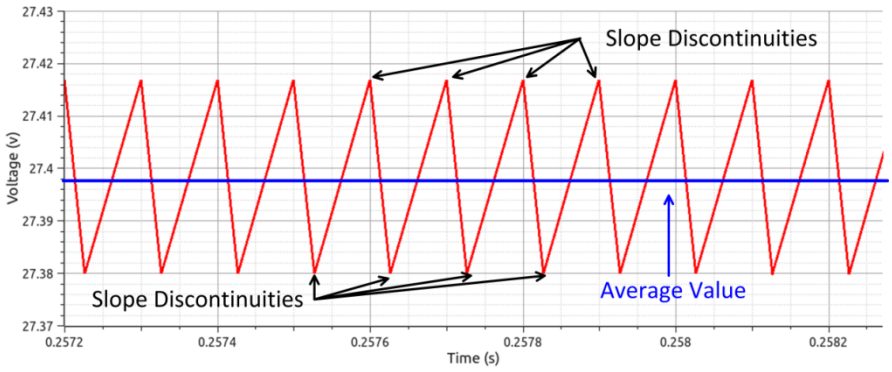

Model discontinuities make its numerical solutions difficult to calculate and the use of more CPU time. Also, analytical solutions for a discontinuous model are difficult to deduce and analyze. In this sense, the average model allows to simplify the system analysis and simulation (Zhang et al, 2016), by considering only the average values of the variables and disregarding their ripples. It is equivalent to replace each variable with its Fourier series and retain only its DC or average components (Qin H and Kimball J.W. (2011). By applying this procedure to equations (5) and (6), the large-signal average model for the boost converter is obtained:

$$L\frac{d\langle i_L\rangle}{dt} = \langle v_i\rangle \cdot \langle u\rangle + [\langle v_i\rangle - \langle v_c\rangle](1-\langle u\rangle) \tag{7}$$

$$C\frac{d\langle v_c\rangle}{dt} = -\frac{\langle v_c\rangle}{R}\cdot\langle u\rangle + \left[\langle i_L\rangle - \frac{\langle v_c\rangle}{R}\right](1-\langle u\rangle) \tag{8}$$

Where $\langle i_L \rangle, \langle v_i \rangle, \langle v_C \rangle$ and $\langle u \rangle$ represents the average values of the original variables. It is important to remark that the $\langle u \rangle$ is not a discrete variable in contrast to u, being possible any value in the range [0,1], as shown in Figure 3.

Figure 3

PWM signal, comparing u and $\langle u \rangle$ variables

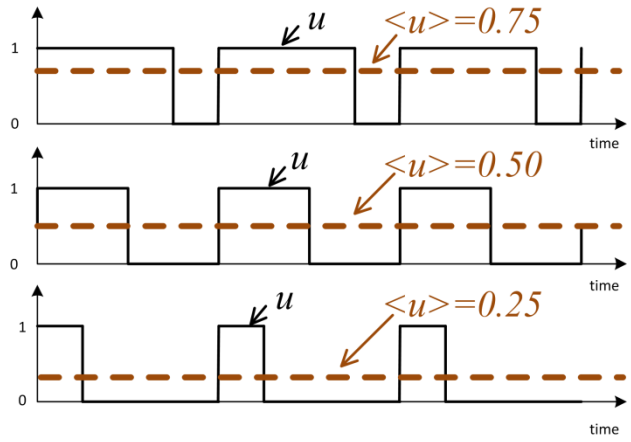

2.3. Step 3: Average model linearization

Even after averaging, the differential equations system of equations (7) and (8) are still non-linear. A linearization process is necessary to obtain a set of linear models, each of them being valid under certain operation conditions of the converter.

Model linearization allows evaluating system behavior when variables experiment small changes near to a fixed operation point, this is called small-signal model (Middlebrook, 1988). The following variables are defined:

$$\langle u_g \rangle = \langle u \rangle - \langle \overline{U} \rangle \quad (9)$$

$$\langle i_{Lg} \rangle = \langle i_L \rangle - \langle \overline{I_L} \rangle \quad (10)$$

$$\langle v_{ig} \rangle = \langle v_i \rangle - \langle \overline{V_i} \rangle \quad (11)$$

$$\langle v_{cg} \rangle = \langle v_c \rangle - \langle \overline{V_c} \rangle \quad (12)$$

Were $\langle u \rangle, \langle i_L \rangle, \langle v_i \rangle, \langle v_c \rangle$ represent the actual values of the converter. $\langle \overline{U} \rangle, \langle \overline{I_L} \rangle$, $\langle \overline{V_i} \rangle$ and $\langle \overline{V_c} \rangle$ represent their operation point fixed values and $\langle u_g \rangle, \langle i_{Lg} \rangle, \langle v_{ig} \rangle, \langle v_{cg} \rangle$represent their small signal deviations.

A small-signal model can be used to predict the system behavior when variables change slightly from its operation point. Such model can be obtained by using the Jacobian linearization (Urrea-Quintero, *et al.*, 2018) that correspond to the partial derivatives of the system to obtain linear relationships in the operation point among all their variables.

The Jacobian linearization starts from an expression of the form:

$$\frac{dx}{dt} = f(x, x_1, x_2, \dots x_n) \tag{13}$$

That expression can be linearly approximated as follows:

$$\frac{dx_g}{dt} \approx Ax_g + A_1 x_{1g} + \cdots + A_n x_{ng} \tag{14}$$

Where:

$$A = \left.\frac{\partial f}{\partial x}\right|_{x=\bar{X},\ x_1=\bar{X_1}\dots x_n=\bar{X_n}} \quad A_1 = \left.\frac{\partial f}{\partial x_1}\right|_{x=\bar{X},\ x_1=\bar{X_1}\dots x_n=\bar{X_n}} \quad \dots \quad A_n = \left.\frac{\partial f}{\partial x_n}\right|_{x=\bar{X},\ x_1=\bar{X_1}\dots x_n=\bar{X_n}} \tag{15}$$

In equations (13), (14) and (15); $\bar{X}$ represents the variable's operation point and x_g their slight deviations from the operation point.

Linearization is applied to equation (7). First, equation (7) is rewritten, please see equation (16). Second, the partial derivatives are calculated and evaluated in the operation point (equations (17), (18) and (19)). Finally, the linearized expression is found in equation (20):

$$\frac{d\langle i_L\rangle}{dt} = f(\langle v_i\rangle, \langle v_C\rangle, \langle u\rangle) = \frac{\langle v_i\rangle \cdot \langle u\rangle + [\langle v_i\rangle - \langle v_C\rangle](1 - \langle u\rangle)}{L} \tag{16}$$

$$\frac{\partial f}{\partial \langle v_i\rangle} = \frac{\langle u\rangle + (1 - \langle u\rangle)}{L} = \frac{1}{L} \rightarrow \left.\frac{\partial f}{\partial \langle v_i\rangle}\right|_{\langle v_i\rangle=\langle \bar{v}_i\rangle,\ \langle v_C\rangle=\langle \bar{v}_C\rangle,\ \langle u\rangle=\langle \bar{U}\rangle} = \frac{1}{L} \tag{17}$$

$$\frac{\partial f}{\partial \langle v_c\rangle} = \frac{-(1 - \langle u\rangle)}{L} \rightarrow \left.\frac{\partial f}{\partial \langle v_c\rangle}\right|_{\langle v_i\rangle=\langle \bar{v}_i\rangle,\ \langle v_C\rangle=\langle \bar{v}_C\rangle,\ \langle u\rangle=\langle \bar{U}\rangle} = -\frac{1 - \langle \bar{U}\rangle}{L} \tag{18}$$

$$\frac{\partial f}{\partial \langle u\rangle} = \frac{\langle v_i\rangle - [\langle v_i\rangle - \langle v_C\rangle]}{L} \rightarrow \left.\frac{\partial f}{\partial \langle v_c\rangle}\right|_{\langle v_i\rangle=\langle \bar{v}_i\rangle,\ \langle v_C\rangle=\langle \bar{v}_C\rangle,\ \langle u\rangle=\langle \bar{U}\rangle} = -\frac{\langle \bar{V}_c\rangle}{L} \tag{19}$$

$$\frac{d\langle i_{Lg}\rangle}{dt} = \frac{1}{L}\langle v_{ig}\rangle - \frac{1 - \langle \bar{U}\rangle}{L}\langle v_{cg}\rangle + \frac{\langle \bar{V}_c\rangle}{L}\langle u_g\rangle \tag{20}$$

Analogously, applying the linearization method to equation (8) yields:

$$\frac{d\langle v_{cg}\rangle}{dt} = -\frac{1}{RC}\langle v_{cg}\rangle + \frac{1 - \langle \bar{U}\rangle}{C}\langle i_{Lg}\rangle - \frac{\langle \bar{I}_L\rangle}{C}\langle u_g\rangle \tag{21}$$

Remember that $\langle \bar{U}\rangle, \langle \bar{I}_L\rangle$ $\langle \bar{V}_i\rangle$ and $\langle \bar{V}_c\rangle$ are constants that depends only of the fixed operation point. Thus, equations (20) and (21) form a linear differential equation system and it is possible to determine their transfer functions by applying Laplace Transform.

2.4. Step 4: Obtaining transfer functions

Transfer functions allows to known each output of the system given their inputs and are computed through the linear model obtained in the previous step. Being equations (20) and (21) a linear differential equation system, it is possible to use transfer function modeling for a convenient representation. Applying Laplace transform to equations (20) and (21) yields:

$$s\langle i_{L\hat{s}}\rangle = \frac{1}{L}\langle v_{i\hat{s}}\rangle - \frac{1-\langle\overline{U}\rangle}{L}\langle v_{c\hat{s}}\rangle + \frac{\langle\overline{V_c}\rangle}{L}\langle u_{\hat{s}}\rangle \quad (22)$$

$$s\langle v_{C\hat{s}}\rangle = -\frac{1}{RC}\langle v_{c\hat{s}}\rangle + \frac{1-\langle\overline{U}\rangle}{C}\langle i_{L\hat{s}}\rangle - \frac{\langle\overline{I_L}\rangle}{C}\langle u_{\hat{s}}\rangle \quad (23)$$

The Boost converter model has two input variables: Duty cycle and input voltage, and two outputs: Inductor current and capacitor voltage. Thus, it is possible to obtain transfer functions from any of the inputs to any of the outputs. This paper focuses on duty cycle input, obtaining transfer functions from duty to inductor current and capacitor voltage. Thus, a constant input voltage must be assumed, that implies there are no deviations from its operation point as stated in equation (24).

$$\langle v_i\rangle = constant = \langle\overline{V_i}\rangle \quad \rightarrow \quad \langle v_{i\hat{s}}\rangle = 0 \quad (24)$$

Solving for $\langle v_{C\hat{s}}\rangle$ at equation (23) yields:

$$\langle v_{c\hat{s}}\rangle = \frac{\frac{1-\langle\overline{U}\rangle}{C}\langle i_{L\hat{s}}\rangle - \frac{\langle\overline{I_L}\rangle}{C}\langle u_{\hat{s}}\rangle}{s+\frac{1}{RC}} \quad (25)$$

And replacing equations (24) and (25) into equation (23) yields:

$$s\langle i_{L\hat{s}}\rangle = -\frac{1-\langle\overline{U}\rangle}{L}\left[\frac{\frac{1-\langle\overline{U}\rangle}{C}\langle i_{L\hat{s}}\rangle - \frac{\langle\overline{I_L}\rangle}{C}\langle u_{\hat{s}}\rangle}{s+\frac{1}{RC}}\right] + \frac{\langle\overline{V_c}\rangle}{L}\langle u_{\hat{s}}\rangle \quad (26)$$

Equation (26) shows the relationship between $\langle u_{\hat{s}}\rangle$ and $\langle i_{L\hat{s}}\rangle$, thus it can be rewritten in the form of a transfer function, by doing sum of fractions, as shown in equation (27).

$$Hi(s) = \frac{\langle i_{L\hat{s}}\rangle}{\langle u_{\hat{s}}\rangle} = \frac{\langle\overline{V_c}\rangle Cs + \left[\frac{\langle\overline{V_c}\rangle}{R} + \langle\overline{I_L}\rangle(1-\langle\overline{U}\rangle)\right]}{LCs^2 + \frac{L}{R}s + [1-\langle\overline{U}\rangle]^2} \quad (27)$$

Analogously, it is possible to obtain the transfer function for capacitor voltage against duty cycle shown in equation (28).

$$Hv(s) = \frac{\langle v_{cs} \rangle}{\langle u_s \rangle} = \frac{-\langle \overline{I_L} \rangle Ls + \langle \overline{V_c} \rangle [1 - \langle \overline{U} \rangle]}{LCs^2 + \frac{L}{R}s + [1 - \langle \overline{U} \rangle]^2} \quad (28)$$

It is worth to make some remarks about the above transfer functions: Note that both transfer functions are second order, as expected for a circuit with two energy storage elements. Numerator and denominator polynomial coefficients depend on the fixed operation point ($\langle \overline{V_c} \rangle$, $\langle \overline{I_L} \rangle$, $\langle \overline{U} \rangle$); by this, changing the operation point will affect system zeros and poles and its dynamical response. In other words, there is not a single transfer function that models the system behavior, but an infinity set of transfer functions which provide a good approximation for a given operating point.

2.5. Step 5: Pole and Zero location analyses

Pole and Zero location analyses are applied over transfer functions which provide the basis for determining the system response characteristics without solving the large-signal model. As it can be seen in equations (27) and (28), the denominator polynomial is the same for $Hi(s)$ and $Hv(s)$. That implies that both transfer functions have the same poles for a given operation point. Poles (P_1, P_2) can be calculated by using the quadratic equation:

$$P_1, P_2 = \frac{-\frac{L}{R} \pm \sqrt{\frac{L^2}{R^2} - 4LC[1 - \langle \overline{U} \rangle]^2}}{2LC} \quad (29)$$

Note that pole location strongly depends on the $\langle \overline{U} \rangle$ parameter. From equation (29) different type of poles (real and different, real and equal, complex conjugate) can be obtained by varying the operation point. Table 1 is obtained by discriminate analysis in equation (29) and resumes the possible pole types.

Table 1
Possible pole types

Real and different poles	$\frac{L^2}{R^2} - 4LC[1 - \langle \overline{U} \rangle]^2 > 0$
Real and equal poles	$\frac{L^2}{R^2} - 4LC[1 - \langle \overline{U} \rangle]^2 = 0$
Complex conjugate poles	$\frac{L^2}{R^2} - 4LC[1 - \langle \overline{U} \rangle]^2 < 0$

In the specific case of complex conjugate poles, their real and imaginary parts are shown in equation (30). Note that the real part does not depend on the operation point ($\langle \overline{U} \rangle$); but only on the resistor and capacitor values. Instead, its imaginary part decreases as $\langle \overline{U} \rangle$ increases. This is important due to the dependency of the transient response parameters in complex pole locations, where its real part is related to stabilization time and its imaginary part is related to oscillation pseudo-period.

$$P_1, P_2 = -\frac{1}{2RC} \pm j\sqrt{\frac{[1-\langle\overline{U}\rangle]^2}{LC} - \frac{1}{4R^2C^2}} \quad (30)$$

Zeros location are different for $Hi(s)$ and $Hv(s)$ functions. Equation (31) yields zero location for current transfer function $Hi(s)$, while equation (32) yields zero location for voltage transfer function $Hv(s)$. In this case, both zeros are strongly dependent on the operation point variables. Note that the zero of $Hv(s)$ is positive, this is indicative of a non-minimal phase behavior for $Hv(s)$.

$$Z_1 = -\frac{\left[\frac{\langle\overline{V_c}\rangle}{R} + \langle\overline{I_L}\rangle(1-\langle\overline{U}\rangle)\right]}{\langle\overline{V_c}\rangle C} \quad (31)$$

$$Z_1 = \frac{\langle\overline{V_c}\rangle[1-\langle\overline{U}\rangle]}{\langle\overline{I_L}\rangle} \quad (32)$$

2.6. Step 6: Steady state relationships

As stated before, the operation point mean values of ($\langle\overline{V_i}\rangle, \langle\overline{V_c}\rangle, \langle\overline{I_L}\rangle, \langle\overline{U}\rangle$) are required for transfer function deduction; however, not any combination of these values is valid because they must reflect a valid stabilization point from the system.

In order to obtain expression for these mean values, equations (7) and (8) are evaluated in the operation point. Also, its time derivatives are set equal to zero to seek for stabilization points. This yields equations (33) and (34):

$$0 = \langle\overline{V_i}\rangle \cdot \langle\overline{U}\rangle + [\langle\overline{V_i}\rangle - \langle\overline{V_c}\rangle](1-\langle\overline{U}\rangle) \quad (33)$$

$$0 = -\frac{\overline{V_c}}{R} \cdot \langle\overline{U}\rangle + \left[\langle\overline{I_L}\rangle - \frac{\langle\overline{V_c}\rangle}{R}\right] \cdot (1-\langle\overline{U}\rangle) \quad (34)$$

Rearranging equations (33) and (34):

$$\langle\overline{V_c}\rangle = \frac{\langle\overline{V_i}\rangle}{1-\langle\overline{U}\rangle} \quad (35)$$

$$\langle\overline{I_L}\rangle = \frac{\langle\overline{V_c}\rangle}{R[1-\langle\overline{U}\rangle]} \quad (36)$$

In this case, equation (35) is the input voltage to output voltage relationship for a Boost converter in steady state. For a given $\langle\overline{V_i}\rangle$ and $\langle\overline{U}\rangle$ it is possible to calculate all the steady state mean values.

2.7. Step 7: OpenModelica Simulation

At this step, OpenModelica capabilities for multi-domain simulation are used to validate the models deduced in previous steps (Murad *et al*., 2017; Reid, 2015). For this, two different models are implemented for the boost converter: One based on electric components (schematic capture) and one based on the transfer functions which correspond to equations (27) and (28).

Figure 4 shows the model built using electric components from OpenModelica ideal elements library. The Boost topology is made of ideal diode, capacitor, inductor, resistor and voltage source. Also, the *Vin_constant* block sets a fixed voltage of the *Vin* source and the PWM block generates the switching signal for the controlled voltage switch.

Figure 4
Boost converter model for simulation, using electric components.

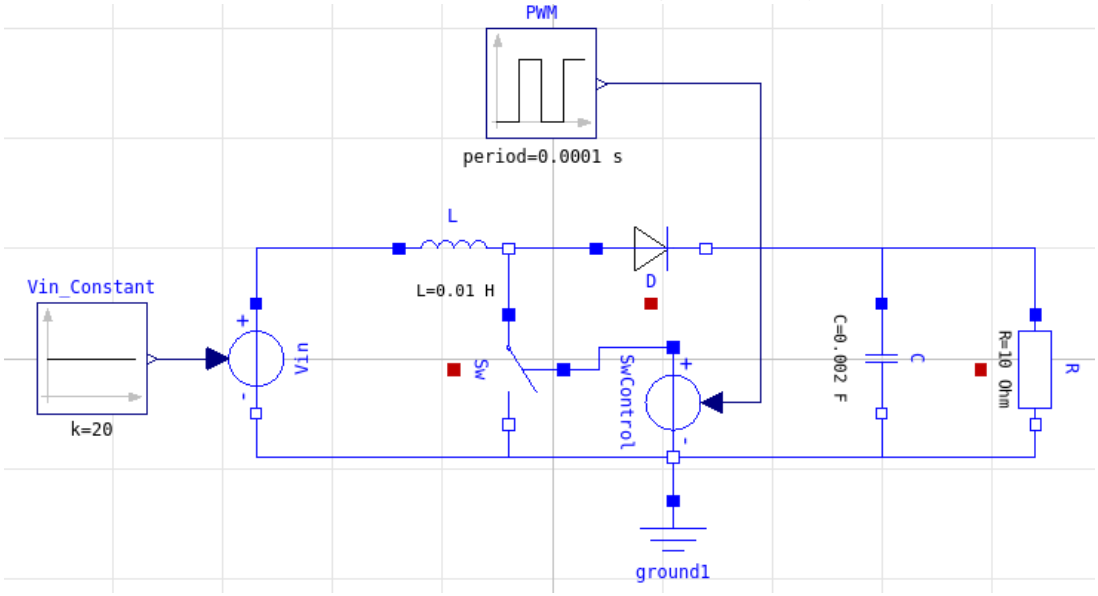

The next considerations are necessary to simulate a small signal step change on duty cycle $\langle u_g \rangle$ near to a fixed operation point $\langle \overline{U} \rangle$ using the electric components model: First, the initial conditions of capacitor voltage and inductor current must be set to $\langle \overline{V_C} \rangle$ and $\langle \overline{I_L} \rangle$, respectively (calculated using the $\langle \overline{U} \rangle$ value of equations (35) and (36)) in order to simulate system stabilization in the operation point. Second, PWM duty cycle is set to $\langle u \rangle = \langle \overline{U} \rangle + \langle u_g \rangle$ were $\langle u_g \rangle$ corresponds to the height of the step change. Third, responses for capacitor voltage and inductor current are registered.

Figure 5 shows the model built using transfer functions; these are indicated in blocks for capacitor voltage $Hv(s)$ (*tf_Voltage*) and inductor current $Hi(s)$ (*tf_Current*). For a fixed operation point, the two transfer functions are defined by using its polynomial coefficients (calculated with equations (27) and (28)). Also, there is a step signal generator configured to generate a $\langle u_g \rangle$ step height. Finally, the adder blocks in the outputs of the transfer functions allow translating the small signal outputs ($\langle v_{cg} \rangle$, $\langle i_{Lg} \rangle$) to the real voltage and current values ($\langle v_c \rangle = \langle v_{cg} \rangle + \langle \overline{V_c} \rangle$, $\langle i_L \rangle = \langle i_{Lg} \rangle + \langle \overline{I_L} \rangle$). *VOperationPoint* and *IOperationPoint* are constant blocks representing $\langle \overline{V_c} \rangle$ and $\langle \overline{I_L} \rangle$, respectively.

A key concept for comparing transfer functions with electric model results is to remember which types of variables are involved in each model. Transfer function involves averaged small-signal variables ($\langle v_{cs} \rangle$, $\langle i_{Ls} \rangle$) while the electric model involves full-signal variables (v_c, i_L). An appropriate translation between these variables is crucial for a successful comparison.

Figure 5
Small-signal boost converter models for simulation, using transfer functions.

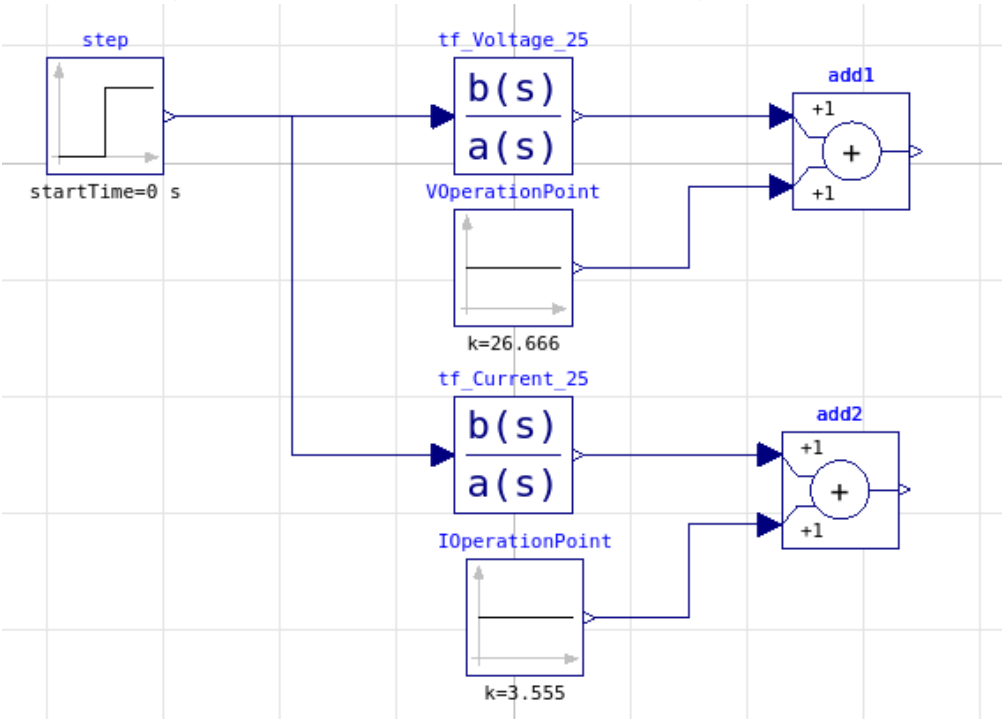

2.8. Summary of the proposed methodology

This section highlights the key aspects of the proposed methodology. The first step is the deduction of the large signal model that permits to obtain the set of differential equations which model the PEC; in this step, all dynamics of the PEC can be observed (fast and slow dynamics). The second step is the deduction of the average model, average model disregards variables ripples and eliminates the fast dynamics; however, it is useful since it allows knowing the nominal values where the system is stabilized. The third step consists on a Jacobian linearization to obtain the small-signal model in a fixed operation point. The small-signal model can be used to predict the system behavior for small changes of variables from its operation point. The fourth step consists on getting the transfer functions which can be obtained if Laplace transform is applied over the small-signal model. These functions are used to obtain each output of the system given their inputs. The fifth step is the pole and zero location analyses which are applied over the transfer functions for obtaining the system responses. Pole analysis is used to estimate the stabilization time and oscillation pseudo-period while zero analysis identifies if any variable of the system has or not non-minimal phase behavior. The sixth step consists on establishing the steady state behavior of the PEC for seeking stabilization points. For obtaining the steady state, derivatives in the average model are equaled to zero and then the required mathematical manipulations are performed to obtain steady state relationships. The seventh step implements through simulation the transfer function model (linear model) and the model based on electric components (non-linear model), this step permits to compare between the linear and non-linear models.

3. Simulation results

A boost converter with the following specifications is considered: L=10 mH, $C = 2000\mu F$, $R = 10\Omega$, $f_{sw} = 10KHz$ and $v_i = 20V$. The simulation was carried out using the default compiler and solver in OpenModelica connection editor (OMEdit), version 3.2.2.

3.1. Exploring converter non-linearity

In this section, the electric components model described in section 2.7 is used to illustrate the non-linear nature of the converter. For an ideal Linear Time Invariant system (LTI system) with zero initial conditions, if the input signal is scaled, the output signal is also scaled by the same value; that is, the output waveform shape is conserved and only its values are altered. Considering the duty cycle of the u signal as the input to the converter (maintaining the input voltage unaltered), it is possible to evaluate this property.

Figure 6 shows the capacitor voltage for different duty cycles, assuming zero initial conditions. It is evident that duty cycle value has a great impact on waveform shape. Note that response at 75% duty present less oscillations before reaching its steady state compared against the 50% and 25% responses. This confirms that duty cycle value has an enormous impact on transient response specifications of the converter. Being the duty cycle the control action for the converter, this dependence creates additional challenges during control systems design, sometimes being necessary the implementation of nonlinear control techniques. Note that this system does not comply with the scaling property of a linear system, thus it can be classified as non-linear.

Figure 6
Large-signal responses for capacitor voltage.
Red: Duty cycle = 25%, Blue: Duty cycle = 50%, Green: Duty cycle = 75%

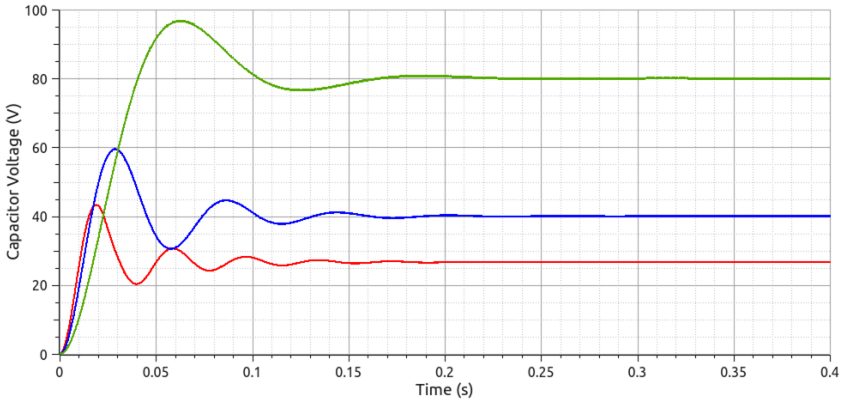

3.2. Transfer functions and pole-zero analysis

Different operation points were considered to evaluate consistence between transfer functions and the converter dynamics through simulation. Specifically, 25%, 50% and 75% duty cycle operation points $(\langle \bar{U} \rangle)$ were used. For each point, $\langle \bar{V}_c \rangle$ and $\langle \bar{I}_L \rangle$ were calculated using equations (35) and (36) (remember, $v_i = \langle \bar{V}_i \rangle = 20V$). Also, the different transfer functions were calculated by using equations (27) and (28). Table 2 shows the operating points and their corresponding transfer functions. As stated before, pole and zero locations depend on the chosen operating point. Figure 7 shows the pole zero diagrams for the transfer functions of Table 2. It can

be seen that pole locations are the same for capacitor voltage and inductor current functions for a given operation point. Poles are complex conjugate at every operation point, their real part is constant but their imaginary part decreases when the operation point duty cycle increases. This corresponds with the discussion of section 2.5 and implies differences on the transient response of the converter when its duty cycle operating point $\langle \bar{U} \rangle$ is changed.

Table 2
Transfer functions for different operation points.

Duty	Operating point	Transfer Functions
$\langle \bar{U} \rangle = 25\%$	$\langle \bar{V_C} \rangle = 26.667$ $\langle \bar{I_L} \rangle = 3.556$	$Hv(s) = \frac{-0.0356s + 20}{20x10^{-6}s^2 + 0.001s + 0.5625}$ $Hi(s) = \frac{0.0533s + 5.3333}{20x10^{-6}s^2 + 0.001s + 0.5625}$
$\langle \bar{U} \rangle = 50\%$	$\langle \bar{V_C} \rangle = 40$ $\langle \bar{I_L} \rangle = 8$	$Hv(s) = \frac{-0.08s + 20}{20x10^{-6}s^2 + 0.001s + 0.25}$ $Hi(s) = \frac{0.08s + 8}{2x10^{-6}s^2 + 0.001s + 0.25}$
$\langle \bar{U} \rangle = 75\%$	$\langle \bar{V_C} \rangle = 80$ $\langle \bar{I_L} \rangle = 32$	$Hv(s) = \frac{-0.32s + 20}{20x10^{-6}s^2 + 0.001s + 0.0625}$ $Hi(s) = \frac{0.16s + 16}{20x10^{-6}s^2 + 0.001s + 0.0625}$

Figure 7
Pole-zero diagrams for transfer functions of Table 2

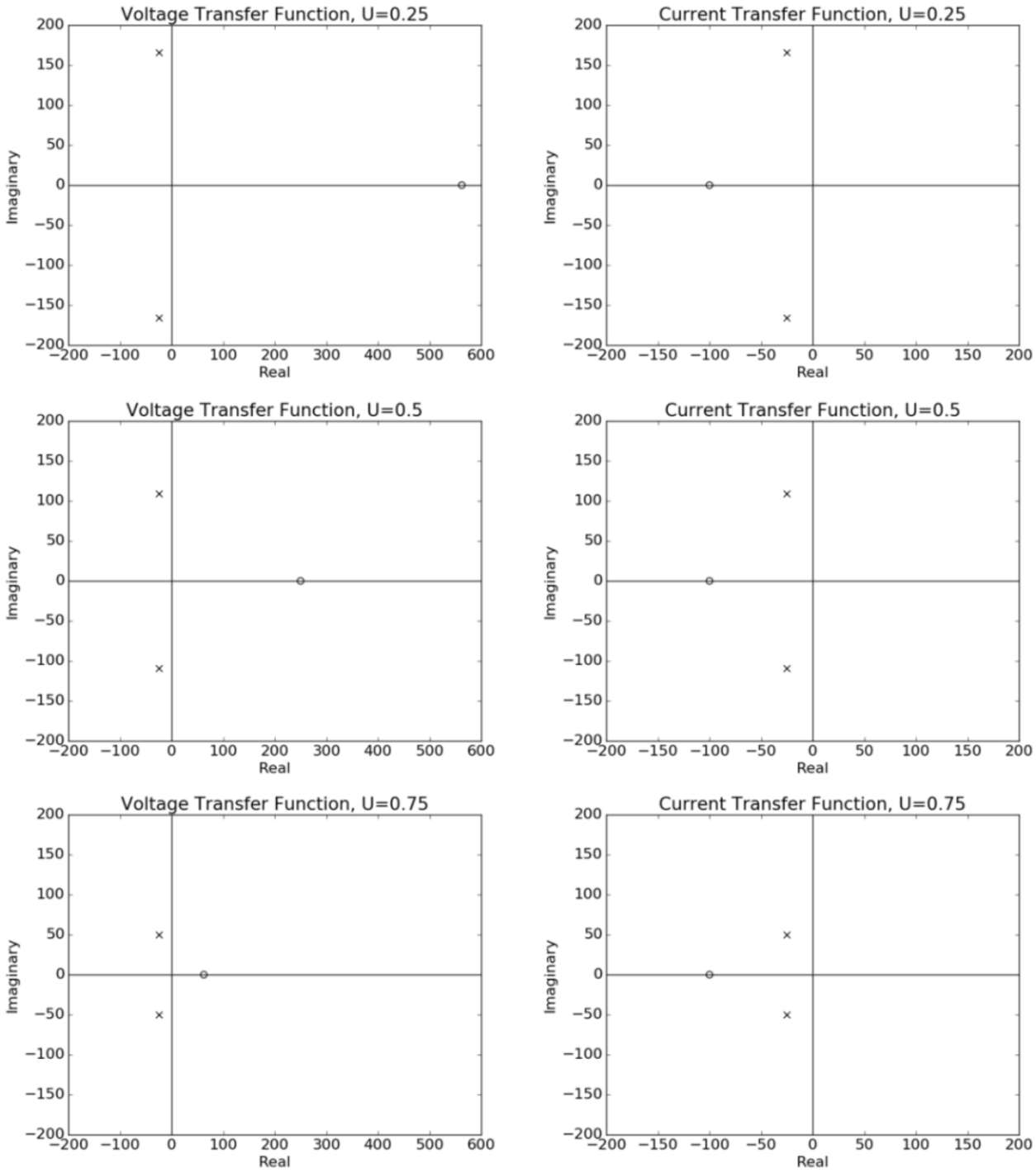

Also note that voltage transfer function has a positive real zero for all operation points. This zero configures a non-minimal phase system (Qui et al, 1993). If a positive step input is applied to this system, the output variable tends to become negative, before changing direction and searching its positive stabilization point. This "undershot" affects the controller action, being necessary to consider it during controller selection and design (Villaroel et al, 2019, Cajamarca et al, 2019, Siddhartha et al, 2019). Instead, the current transfer function has a negative real zero and its position does not depend of the operating point.

3.2. Comparison between transfer function and converter responses

Figures 8 to 10 show the comparison results using the transfer functions and operation points calculated in Table 2, using the methodology described in section 2.7. A step height $(u_g) = 0.01 = 1\%$ is assumed for all simulations:

Figure 8
Voltage and current responses for 25% of duty cycle,
red: electric model, blue: transfer function.

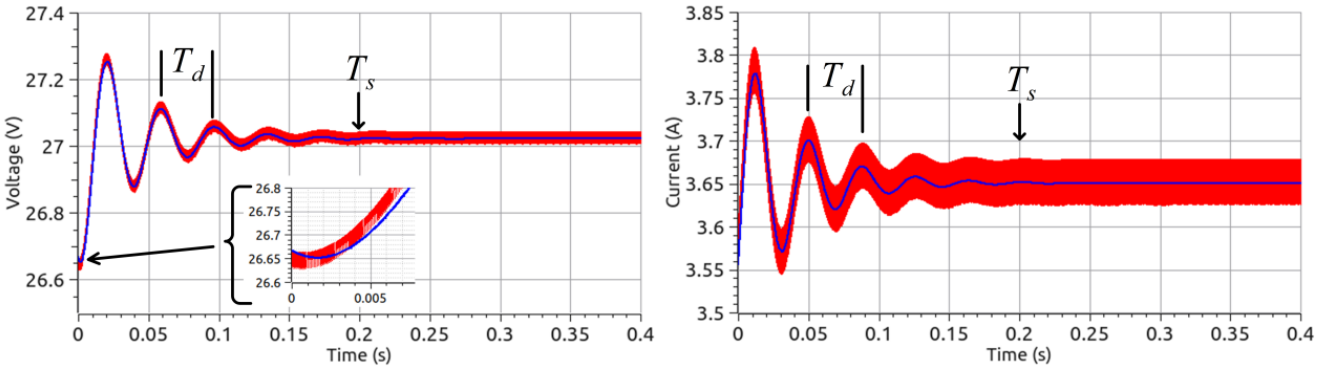

Figure 9
Voltage and current responses for 50% of duty cycle,
red: electric model, blue: transfer function.

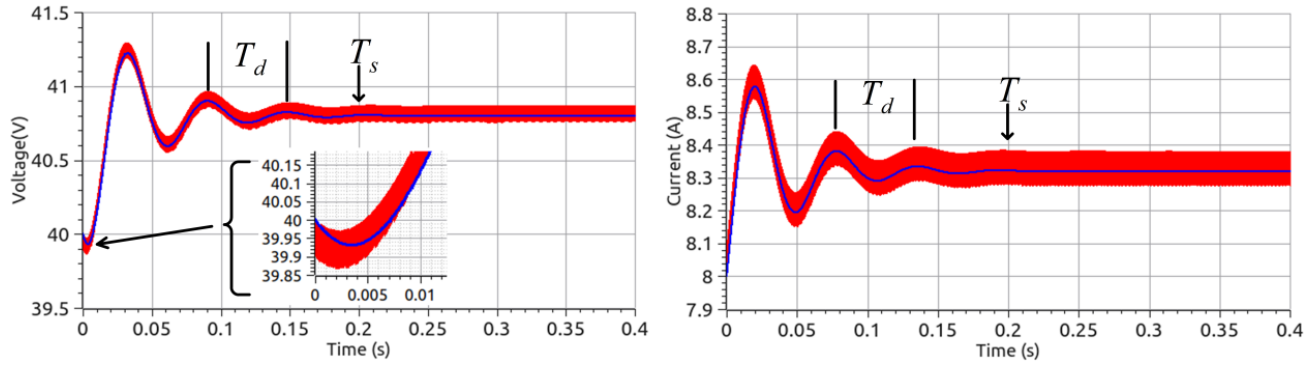

Figure 10
Voltage and current responses for 75% of duty cycle,
red: electric model, blue: transfer function.

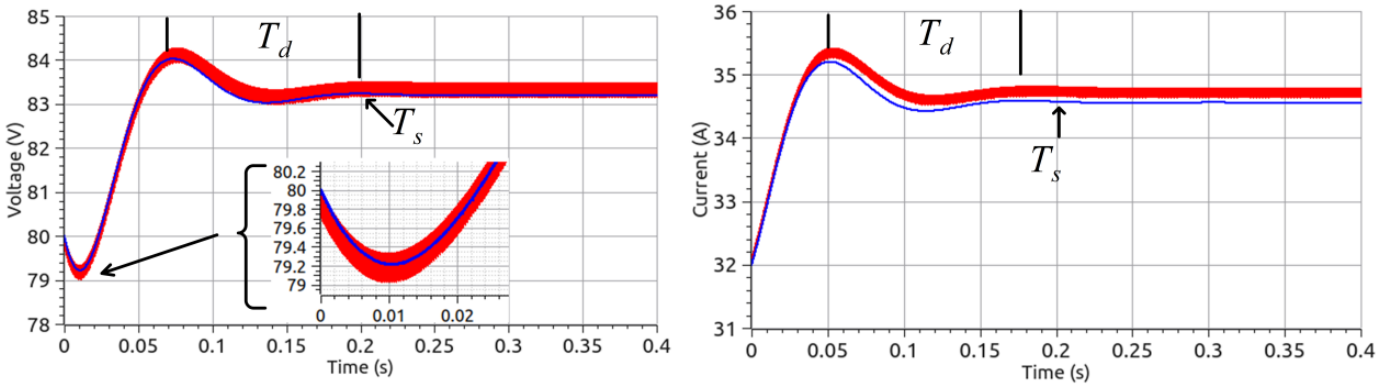

An evident difference between the transfer function and the electric model responses is the signal ripple. It is absent on transfer functions responses. Note that transfer functions were deduced by taking as basis the average

model described in section 2.2, this is why they do not include commutation ripple. However, it can be seen that transfer functions are good approximations for converter behavior considering both transient response and steady state value. These validate the linearization procedure proposed in this paper.

It is worth to mention that there are significant changes in the converter response when the operation point is changed. All responses are under-damped and have equal stabilization times; however, their pseudo-periods are different, please see Table 3. This is congruent with the pole analysis described before where the real part of the poles (associated to stabilization time) is not affected by the operation point but the imaginary one (associated to pseudo-frequency) is decreased as duty cycle operation point increases. Pseudo periods (T_d) and stabilization times (T_s) where indicated at figures 8 to 10.

Table 3
Transient response metrics for capacitor voltage signals.

	$\langle \bar{U} \rangle = 25\%$	$\langle \bar{U} \rangle = 50\%$	$\langle \bar{U} \rangle = 75\%$
Pseudo-period (T_d)	37.89ms	57.67ms	125.67ms
Stabilization time (T_s)	200ms	200ms	200ms

The non-minimal phase characteristic of voltage transfer function can be observed in figures 8 to 10. Note that the step input is positive for all cases, but the voltage output initially decreases before inverting its tendency and starting to increase (due to the positive zero on the transfer function). This effect is more evident in high duty cycle operation points (figure 10). In this case, the current responses do not show this effect, as expected by not having a positive zero.

It is interesting to explore how the errors between transfer functions and electrical model responses grow when the input step becomes larger. Figure 11 shows output voltage responses at a fixed operation point of $\langle \bar{U} \rangle = 25\%$ and changing the step height $\langle u_\delta \rangle = 0.5\%, 1\%, 2\%$. It can be observed that at $\langle u_\delta \rangle = 0.5\%$ (blue signal for transfer function and red signal for electric model) and $\langle u_\delta \rangle = 1\%$ (light blue signal for transfer function and violet signal for electric model) there is a good match between the transfer function and the electric model. However, in $\langle u_\delta \rangle = 2\%$ (black signal for transfer function and light green signal for electric model) differences become evident for transfer function response: in the transient state there is a shorter pseudo-period, and its steady state value is slightly low. It is indicative of how transfer function approximation worsens as the deviation from operation point increases.

Figure 11

Different capacitor voltage step responses for $\langle \bar{U} \rangle = 25\%$ and: $\langle u_\delta \rangle = 0.5\%$ (red: electric model, blue transfer function), $\langle u_\delta \rangle = 1\%$ (violet: electric model, light blue transfer function) and $\langle u_\delta \rangle = 2\%$ (light green: electric model, black: transfer function).

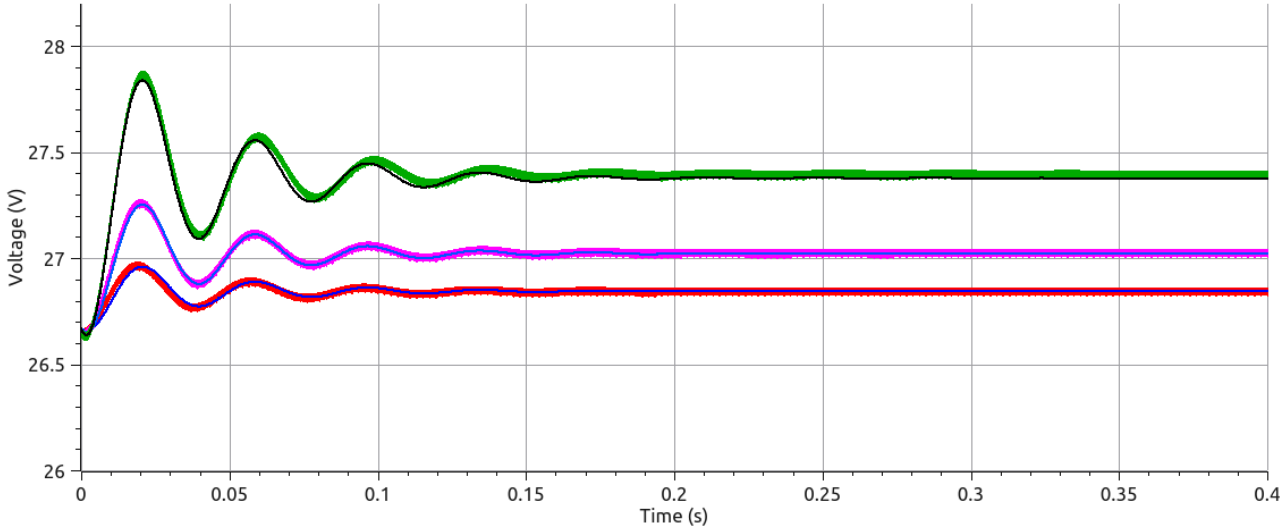

The last analysis can be repeated in a different operation point. Figure 12 shows the results for $\langle \bar{U} \rangle = 75\%$ using the same step heights ($\langle u_\delta \rangle = 0.5\%, 1\%, 2\%$) and signal colors from figure 11. In this operation point, it is more evident the voltage error for $\langle u_\delta \rangle = 2\%$, during its transient and steady states. Instead, in $\langle u_\delta \rangle = 0.5\%$ and 1% there is a good approximation between transfer function and electric model responses. Note that the range of $\langle u_\delta \rangle$ that allows a good approximation depends on the operation point.

Figure 12

Different capacitor voltage step responses for $\langle \bar{U} \rangle = 75\%$ and: $\langle u_\delta \rangle = 0.5\%$ (red: electric model, blue transfer function), $\langle u_\delta \rangle = 1\%$ (violet: electric model, light blue transfer function) and $\langle u_\delta \rangle = 2\%$ (light green: electric model, black: transfer function).

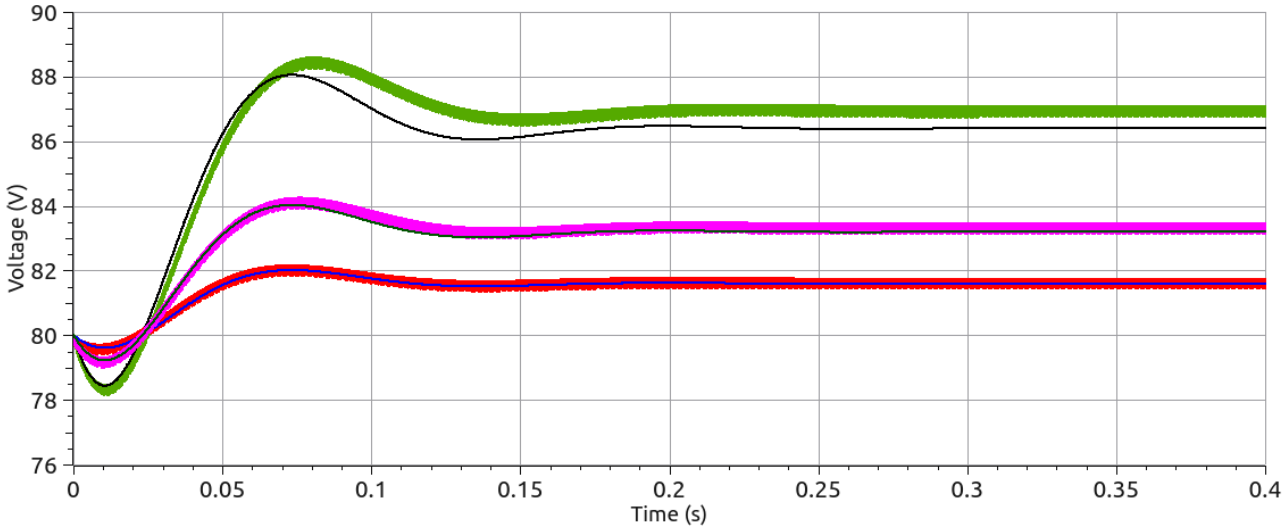

4. Conclusions

PECs are non-linear systems that can be approximated by a set of transfer functions which depend on the operation point. In this paper, a step-by-step methodology of the linearization process of a PEC is presented and validated by using simulation. Results clearly show the non-linear behavior of the DC/DC Boost converter, the following aspects are highlighted: 1) Duty cycle value has a great impact on waveform shape; if duty cycle is increased, the waveform has less oscillations before reaching its steady state. 2) Poles are equal for both voltage and current transfer functions. For the converter taken into consideration, poles are complex conjugate for each operation point; their real part is constant for different operation points so that stabilization times remain constant not depending on the operation point. The imaginary part decreases when the operation point duty cycle increases which also increases the oscillation pseudo-period. 3) Voltage transfer function has a positive real zero with exhibits the non-minimal phase behavior. When duty is increased, the positive real zero decreases which implies that the non-minimal phase behavior is more evident. 4) It was found that as the deviation from the operation point increases, the transfer function approximation worsens. Also, the range of deviation depends on the operation point, for the same deviation, as duty increases the error between the transfer function and the electric model responses also increases.

Acknowledgment

The authors gratefully acknowledge the support from the Colombia Scientific Program within the framework of the call Ecosistema Científico (Contract No. FP44842- 218-2018). The authors also want to acknowledge Universidad de Antioquia for its support through the project “Estrategia de Sostenibilidad”.

Bibliographic references

Beldjajev, V. and Roasto, I. (2012). Efficiency and Voltage Characteristics of the Bi-Directional Current Doubler Rectifier. Przeglad Elektrotechniczny, 88(8), 124–129.

Bi, Z. and Xia, W. (2010). Modeling and Simulation of Dual-Mode DC/DC Buck Converter. Second International Conference on Computer Modeling and Simulation, Sanya, Hainan (China), 371-375.

Cajamarca, B., Camacho, O., Chávez, D., Leica, P., and Pozo, M. (2019). Sliding Mode Control Based on Internal Model for a Non-minimum phase Buck and Boost Converter. Enfoque UTE, 10(1), 41-53.

Chamas, I., and Nokali, M. E. (2004). Automated PSpice simulation as an effective design tool in teaching power electronics. IEEE Transactions on Education, 47(3), 415-421.

Davoudi, A., Jatskevich, J., Chapman, P. L. and Bidram, A. (2013). Multi-Resolution Modeling of Power Electronics Circuits Using Model-Order Reduction Techniques. IEEE Transactions on Circuits and Systems I: Regular Papers, 60(3), 810–823.

Hinz, H., and Hasimi, M. N. (2018). Using Simulation Tools in Power Electronics Courses—A Case Study. In 2018 IEEE 10th International Conference on Engineering Education (ICEED), Kuala Lumpur (Malaysia)

Middlebrook, R. D. (1988). Small-signal modeling of pulse-width modulated switched-mode power converters. Proceedings of the IEEE, 76(4), 343-354.

Muñoz-Galeano, N., Lopez-Lezama, J.M., and Villada-Duque, F. (2019). Methodology for teaching the buck converter: step by step description of the design. Revista Espacios, 40(44), 2. Recuperado de http://www.revistaespacios.com/a19v40n44/19404402.html

Murad, M. A. A., Vanfretti, L., Rokonuzzaman, M., Tuhin, R. A. (september, 2017). Enhancing engineering studies in developing countries using OpenModelica. In 2017 4th International Conference on Advances in Electrical Engineering, Dhaka (Bangladesh)

Qin, H., and Kimball, J. W. (2011). Generalized average modeling of dual active bridge DC–DC converter. IEEE Transactions on power electronics, 27(4), 2078-2084.

Qiu, L., and Davison, E. J. (1993). Performance limitations of non-minimum phase systems in the servomechanism problem. Automatica, 29(2), 337-349.

Raud, Z., and Vodovozov, V. (2019). Virtual Lab to Study Power Electronics in LabVIEW Framework. In 2019 Electric Power Quality and Supply Reliability Conference (PQ) & 2019 Symposium on Electrical Engineering and Mechatronics (SEEM), Kärdla (Estonia)

Reid, D. (2015). DQ rotating frame PI control algorithm for power inverter voltage regulation modelling and simulation using the OpenModelica platform. In IEEE SoutheastCon 2015, Fort Lauderdale (EEUU)

Rukun, K. (2018). A Review of the Teaching and Learning on Power Electronics Course. In IEEE 2018 International Conference on Applied Information Technology and Innovation (ICAITI), Padang (Indonesia)

Siddhartha, V., and Hote, Y. V. (2019). IMC-PID design of DC-DC converters exhibiting non-minimum phase characteristics. In 2019 IEEE Power and Energy Conference at Illinois (PECI), Champaign (USA)

Urrea-Quintero, JH., Muñoz-Galeano, N., Gómez-Echavarría, LM. (2018). Analysis and Control of Power Electronic Converters Based on a System Zeros Location Approach. In Anh Tuan, L. Applied Modern Control (pp.1-22). London: Intechopen.

Villarroel, F., Espinoza, J., Pérez, M., Ramírez, R., Baier, C., and Morán, L. (2019). Shortest horizon FCS-MPC output voltage tracking in non-minimum phase boost-type converters. In IECON 2019-45th Annual Conference of the IEEE Industrial Electronics Society, Lisbon (Portugal)

Yang, T., Liao, Y. (2019). Discrete Sliding Mode Control Strategy for Start-Up and Steady-State of Boost Converter. Energies, 12(15), 2990.

Zhang, K., Shan, Z., and Jatskevich, J. (2016). Large-and small-signal average-value modeling of dual-active-bridge DC–DC converter considering power losses. IEEE Transactions on Power Electronics, 32(3), 1964-1974.